COMMUNICATION

Energy Storage

ADVANCED
ENERGY
MATERIALS

www.advenergymat.d

Check for
updates

A Phosphonate-Functionalized Quinone Redox Flow Battery at Near-Neutral pH with Record Capacity Retention Rate

Yunlong Ji, Marc-Antoni Goulet, Daniel A. Pollack, David G. Kwabi, Shijian Jin, Diana De Porcellinis, Emily F. Kerr, Roy G. Gordon,* and Michael J. Aziz*

A highly stable phosphonate-functionalized anthraquinone is introduced as the redox-active material in a negative potential electrolyte (negolyte) for aqueous redox flow batteries operating at nearly neutral pH. The design and synthesis of 2,6-DPPEAQ, (((9,10-dioxo-9,10-dihydroanthracene-2,6-diyl) bis(oxy))bis(propane-3,1-diyl))bis(phosphonic acid), which has a high solubility at pH 9 and above, is described. Chemical stability studies demonstrate high stability at both pH 9 and 12. By pairing 2,6-DPPEAQ with a potassium ferri/ferrocyanide positive electrolyte across an inexpensive, nonfluorinated permselective polymer membrane, this near-neutral quinone flow battery exhibits an open-circuit voltage of 1.0 V and a capacity fade rate of 0.00036% per cycle and 0.014% per day, which is the lowest ever reported for any flow battery in the absence of rebalancing processes. It is further demonstrated that the negolyte pH drifts upward upon atmospheric oxygen penetration but, when oxygen is excluded, oscillates reversibly between 9 and 12 during cycling. These results enhance the suitability of aqueous-soluble redox-active organics for use in large-scale energy storage, potentially enabling massive penetration of intermittent renewable electricity.

The dramatic decline in the cost of solar and wind energy has facilitated a dramatic increase in electricity generated from these renewable sources.[1] However, the inherent intermittency of solar and wind energy has impeded their widespread substitution for fossil electricity. Recent years have seen substantial effort to solve this problem by developing cost-effective, safe, and scalable stationary electricity storage. Solid-electrode batteries such as Li-ion batteries are widespread, but their high cost limits their usage in grid-scale systems. Among the most promising solutions are redox-flow batteries (RFBs), which store the electro-active chemical species separately from the power-generating electrode stack, through which the reactants are pumped during operation. This design allows the energy capacity of the entire system to be scaled independently of its maximum power output so that cost-effective long-duration discharge can be achieved.[2]

All-vanadium systems now have the largest market-share among RFBs, but their penetration is limited by the relatively low Earth-abundance and high cost of vanadium.[3] In contrast, the low cost of some organic molecules and the Earth-abundance of carbon offer promising advantages of redox-active organics for massive penetration of grid-scale energy storage.[4] Moreover, the chemical tunability of organic molecules permits improvements in solubility, redox potential, and stability, which can enhance the energy density, power density, and lifetime of a battery.

There have been numerous reports regarding RFB chemistries based on quinone,[4a,c,5] viologen,[4b,6] ferrocene,[6a,c] alloxazine,[4d] nitroxide radical motifs,[4b,7] and phenazine[7c,8] in the past four years which, while demonstrating promising performance, fall short of meeting all of the technical requirements for practical deployment. Due to the generally low chemical stability of these reactants, most existing systems experience high temporal capacity fade rates on the order of 0.1–10% per day, which limits their long-term use and renders most of these chemistries unsuitable for commercialization. Voltage trades off against stability in many cases. This is most readily apparent in cells utilizing substituted viologens against substituted ferrocenes, where adequate stability has been accompanied by large compromises in open-circuit voltage (OCV).[6a,c,d] Recently, we reported a negative electrolyte (negolyte) comprising 4,4-((9,10-anthraquinone-2,6-diyl)dioxy) dibutyrate (2,6-DBEAQ),[9] that combines high chemical stability with an OCV of ≥1.0 V against a potassium ferri/ferrocyanide positive electrolyte (posolyte). This flow battery exhibited a capacity fade rate of 0.04% per day, which was the lowest of any quinone species at the time. In the current work, we report an aqueous RFB employing a phosphonate-functionalized

Dr. Y. Ji, E. F. Kerr, Prof. R. G. Gordon
Department of Chemistry and Chemical Biology
Harvard University
12 Oxford Street, Cambridge, MA 02138, USA
E-mail: gordon@chemistry.harvard.edu
Dr. M.-A. Goulet, Dr. D. G. Kwabi, S. Jin, Dr. D. De Porcellinis,
Prof. R. G. Gordon, Prof. M. J. Aziz
Harvard John A. Paulson School of Engineering and Applied Sciences
29 Oxford Street, Cambridge, MA 02138, USA
E-mail: maziz@harvard.edu
D. A. Pollack
Department of Physics
Harvard University
17 Oxford St, Cambridge, MA 02138, USA

The ORCID identification number(s) for the author(s) of this article can be found under https://doi.org/10.1002/aenm.201900039.
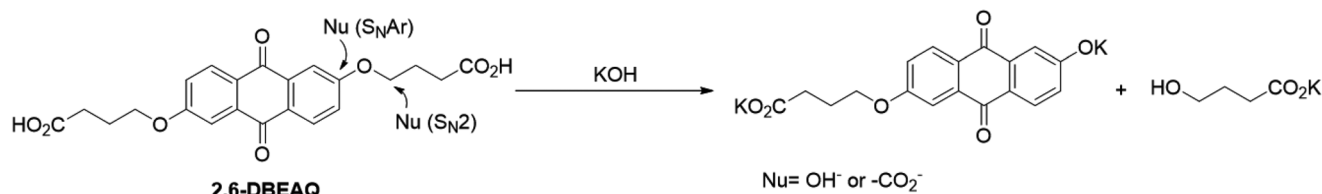
Scheme 1. Proposed decomposition mechanisms for 2,6-DBEAQ.

quinone, (((9,10-dioxo-9,10-dihydroanthracene-2,6-diyl)bis(oxy))bis(propane-3,1-diyl))bis(phosphonic acid) (2,6-DPPEAQ[10]), that sets a new record low capacity fade rate of 0.014% per day in full-cell cycling. These results extrapolate, assuming exponential decay, to a capacity loss of 5.0% per year while undergoing 40 complete charge–discharge cycles per day. The economic tradeoff of the present value of small annual replacements of the active species versus the potential capital cost savings from substituting organic for vanadium favors the organic when the interest rate for discounting is high.[5b] These results also highlight the benefit of studying the stability of organic molecules in both oxidized and reduced redox states to guide active species engineering. We have thus realized high-performance aqueous organic RFBs engineered for lifetime, voltage, power density, and energy density.

In this work, we propose a molecular design to improve chemical stability and battery lifetime based on the decomposition mechanism of the previous frontrunner, 2,6-DBEAQ. Chemical stability studies at elevated temperature indicate that the oxidized form of 2,6-DBEAQ is susceptible to decomposition by γ-hydroxybutyrate cleavage (**Scheme 1**), as confirmed by ^{1}H NMR.[9] Notably, cleavage of a second γ-hydroxybutyrate moiety leads to 2,6-dihydroxyanthraquione (2,6-DHAQ), whose capacity fade rate has been reported as 5% per day.[9,11] The rate of 2,6-DBEAQ decomposition has been shown to be considerably slower at pH 12 relative to pH 14 at 95 °C and 0.1 M concentration (**Figure 1**E,F and Figure S8, Supporting Information).[9] Noting the influence of pH on the degradation rate and that both hydroxide and carboxylate may act as nucleophiles in the decomposition (Scheme 1), we therefore expect further enhancement in stability either by operating at lower pH conditions or by suppressing carboxylate-mediated intramolecular nucleophilic substitution. We designed an analogue of 2,6-DBEAQ with phosphonate-terminated rather than carboxylate-terminated functional groups, 2,6-DPPEAQ, that appears to successfully exploit both of these approaches.

2,6-DPPEAQ was synthesized by the route illustrated in **Scheme 2**, which presents several advantages that render it particularly suitable for large scale industrial manufacturing. The simple synthesis uses only two steps, an O-alkylation reaction and hydrolysis of the ester, to introduce the highly soluble phosphonic acid terminal groups. Both synthesis steps achieved >98% yield, facilitating scale-up without the need for more resource-intensive purification such as chromatography.

Whereas the solubility of 2,6-DBEAQ at pH 9 (<35 mM) is impractically low for use in a cell, the phosphonate functional group affords 2,6-DPPEAQ a much higher solubility at pH 9 (0.75 M, i.e., 1.5 M electrons), enabling the operation of 2,6-DPPEAQ under milder, less strongly basic conditions. When

elevated temperature chemical degradation studies were performed for 2,6-DPPEAQ at pH 9 as well as at pH 12, no significant decomposition was observed in either case (Figure 1A–D). 2,6-DBEAQ and 2,6-DPPEAQ do, however, exhibit a similar extent of decomposition at pH 14 (Figure S8, Supporting Information). The differing relative stabilities of 2,6-DPPEAQ and 2,6-DBEAQ at pH 12 (at 95 °C and 0.1 M concentration), in contrast to the similar extent of their observed decomposition at pH 14, may be due to different decomposition reactions dominating under the different pH conditions. The concentration of hydroxide ions at pH 14 is tenfold higher than the concentration of either molecule at 0.1 M, as opposed to tenfold lower at pH 12. First, we propose that a hydroxide-mediated nucleophilic substitution reaction (S_NAr or S_N2) dominates in the decomposition of both molecules at pH 14. In contrast, we propose that at pH 12, an intramolecular reaction with carboxylate acting as the nucleophile dominates in the decomposition of 2,6-DBEAQ, whereas no analogous intramolecular reaction of 2,6-DPPEAQ is observed at pH 12 due to a much weaker nucleophilicity of the bulky phosphonate group relative to carboxylate.[12] The proposed difference in the mechanisms of 2,6-DBEAQ decomposition at pH 12 and 14 is also consistent with the observation that the initial rate of degradation is not 100-fold slower at pH 12 relative to pH 14. Unlike the oxidized form of 2,6-DPPEAQ, its reduced form, obtained by electrochemical reduction, exhibits robust chemical stability even at pH 14 (Figure S9, Supporting Information). Collectively, these results demonstrate the unprecedented stability of 2,6-DPPEAQ, among quinones, between pH 9 and 12. In addition, the operability at lower pH potentially enables corrosion resistance with less expensive electrolyte-contacting materials.

Based on cyclic voltammetry (CV), 2,6-DPPEAQ exhibits a reversible redox peak at –0.47 V versus a standard hydrogen electrode (SHE) ($E_{1/2}$) in pH 9 unbuffered aqueous solution and at –0.49 V versus SHE ($E_{1/2}$) in pH 12 unbuffered aqueous solution (**Figure 2**A). In contrast, in buffered pH 9 and pH 12 solutions, 2,6-DPPEAQ shows redox potentials of –0.39 versus standard hydrogen electrode (SHE) ($E_{1/2}$) and –0.47 V versus SHE ($E_{1/2}$), respectively (Figure S3, Supporting Information), conforming to the pH-dependent behavior of the reduction potential of quinones in aqueous media.[13] During the cell cycling process, the proton-coupled electron transfer reaction of quinones in water influences the pH, as the reduction of quinones in aqueous solution consumes protons, whereas oxidation of hydroquinones in aqueous solution releases protons. These pH changes should be reversible during cell cycling. To examine the pH reversibility and cycling stability, a cell was assembled with a negolyte comprising 0.1 M of the tetra-potassium salt of 2,6-DPPEAQ in 1 M KCl, the pH of which
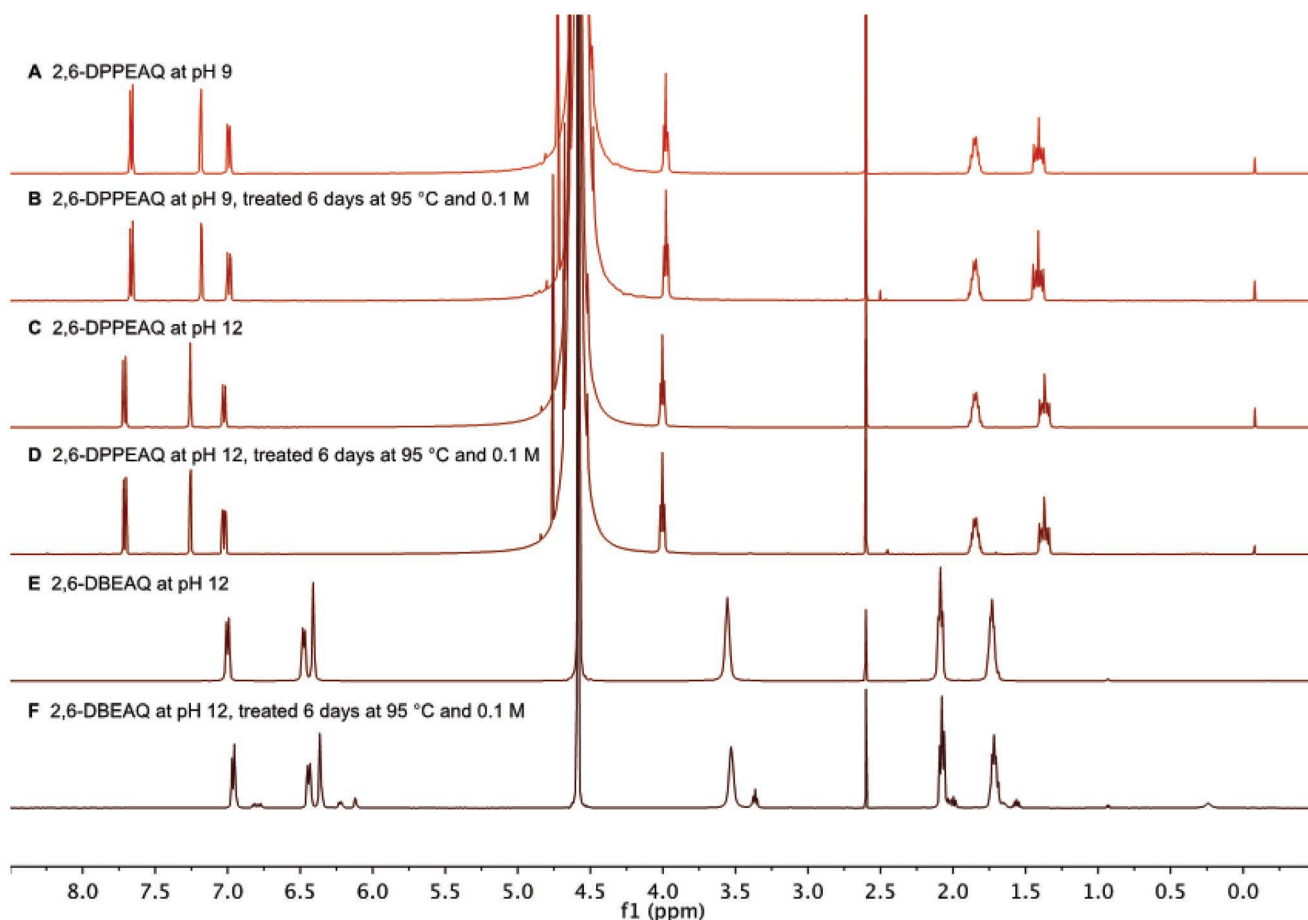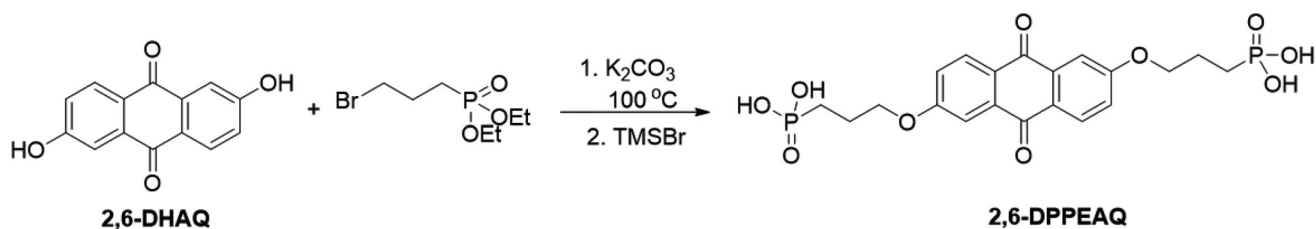
1900039 (2 of 7)

Figure 1. Comparison of the stability of 2,6-DPPEAQ with respect to alkyl chain cleavage at pH 9 and 12 to that of 2,6-DBEAQ at pH 12, all at 0.1 M quinone concentration in aqueous solution. ^{1}H NMR spectra (500 MHz, 10 mM NaCH₃SO₃ internal standard, δ 2.6 ppm) of 2,6-DPPEAQ at pH 9, A) before and B) after treatment for 6 days at 95 °C; 2,6-DPPEAQ at pH 12, C) before and D) after treatment for 6 days at 95 °C; 2,6-DBEAQ at pH 12, E) before and F) after treatment for 6 days at 95 °C. After 95 °C treatment, 2,6-DBEAQ at pH 12 exhibits 15% decomposition, whereas 2,6-DPPEAQ at both pH 9 and pH 12 exhibits no significant decomposition.

was monitored by a pH probe immersed in the solution, and a posolyte comprising 0.1 M K₄Fe(CN)₆ and 0.01 M K₃Fe(CN)₆ in 1 M KCl, separated by a Fumasep E-620 (K) membrane (Figure 2B,C). The pH of both sides was adjusted to 9 by adding a trace amount of KOH. Operating at pH values as low as 9 enhances the stability not only of the negolyte but also of the posolyte, as the decomposition rate of ferricyanide, which is typically used as a posolyte species in alkaline batteries, is increased at high pH.[14] The cell was cycled at a constant current density of ±20 mA cm⁻² for 16 cycles using voltage cut-offs of 0.4 and 1.2 V. During the first charge cycle, the negolyte

pH increased from 9.2 to 12.2. After the first discharge cycle, the pH decreased to 9.9 instead of 9.2. We attribute the increase in pH in the discharged state to the consumption of oxygen present in the solution and reservoir. When hydroquinone is oxidized electrochemically during cell discharge, the increase in pH that occurred during charging is reversible. If, however, hydroquinone, in any protonation state, is instead oxidized by molecular oxygen, then an irreversible increase in pH occurs. In this case, the quinone serves as a mediator for the oxygen reduction reaction (ORR), which has the effect of increasing the pH (see Supporting Information). Subsequent to the first

Scheme 2. Synthetic route for 2,6-DPPEAQ.

**ADVANCED
SCIENCE NEWS**

www.advancedsciencenews.com

**ADVANCED
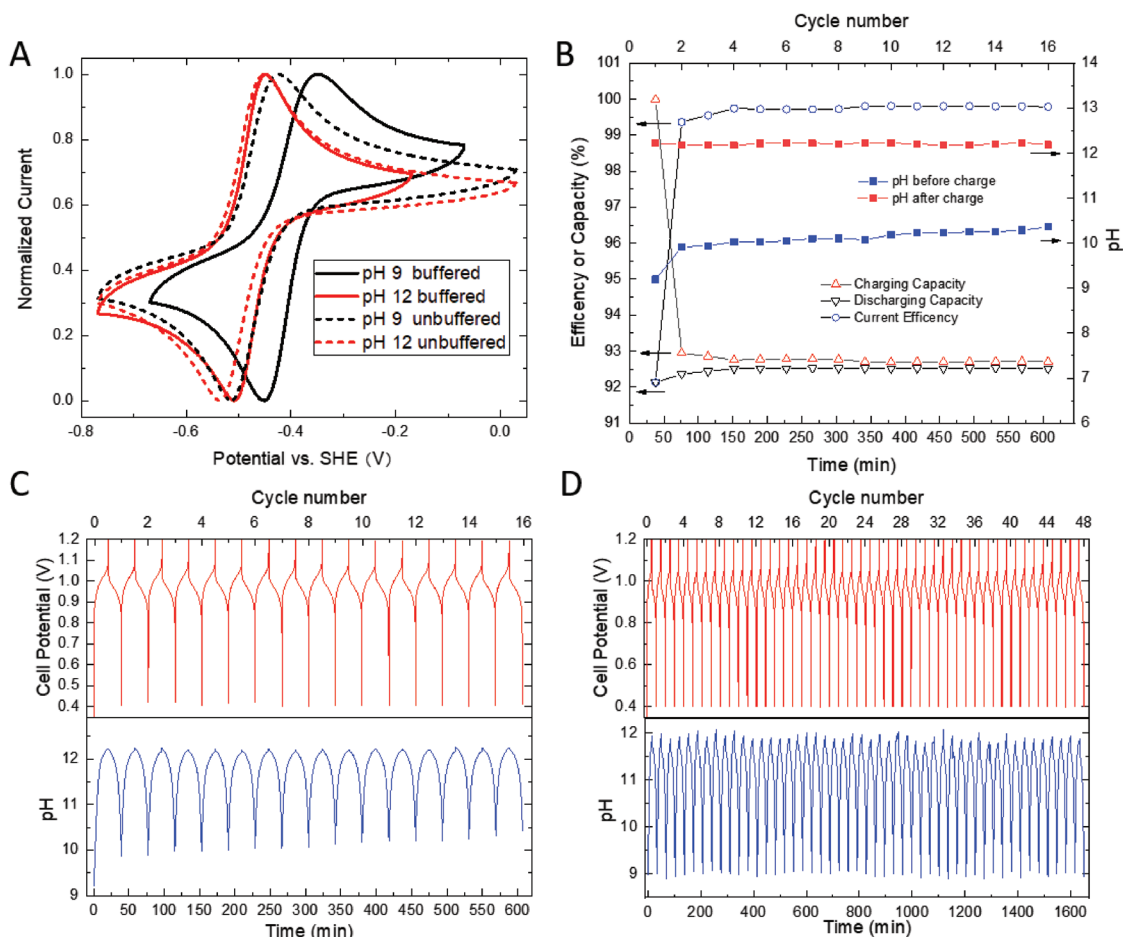ENERGY
MATERIALS**

www.advenergymat.de

Figure 2. A) Cyclic voltammograms of 1 mM 2,6-DPPEAQ at pH 9 buffered solution (black solid), pH 12 buffered solution (red solid), pH 9 unbuffered solution (black dash), and pH 12 unbuffered solution (red dash) at a scan rate of 100 mV s^{-1} on a glassy carbon working electrode. B) Galvanostatic cycling of the 2,6-DPPEAQ cell at 20 mA cm^{-2} for 16 consecutive cycles in a glove bag. Electrolytes comprised 6.5 mL 0.1 M of the tetra-potassium salt of 2,6-DPPEAQ (negolyte) in 1 M KCl solution at pH 9 and 40 mL 0.1 M potassium ferrocyanide and 0.01 M potassium ferricyanide (posolyte) in 1 M KCl solution at pH 9. The pH probe was immersed in the negolyte to monitor the pH of the solution. Charge/discharge capacity, CE, and pH of the negolyte before and after charging are plotted as functions of the cycle number. C) Representative curves of cell potential and negolyte pH versus time. D) Representative curves of cell potential and negolyte pH versus time for the experiment depicted in (B) and (C) repeated in a glove box instead of a glove bag.

cycle, the current efficiency (CE) exceeded 99%, and both the potential and pH cycles exhibited high reproducibility. The negolyte pH oscillated reversibly between ≈10 and 12 during the charge and discharge process. The discharge capacity did not fade perceptibly after 16 cycles (9.5 h), indicating that the battery is capable of operating with minimal capacity fade, consistent with the demonstrated high chemical stability. The negolyte pH in the charged state remained at ≈pH 12.2, suggesting that the redox reaction becomes pH independent at pH values higher than 12.2 (see Supporting Information). In contrast, the negolyte pH in the discharged state continued to slowly increase to 10.4 after 16 cycles (9.5 h), which we attribute to atmospheric oxygen penetration. The posolyte pH remained stable, as the redox reaction of ferri/ferrocyanide does not involve protons. To exclude oxygen penetration causing upward pH drift, another cell was cycled in a glove box instead of a glove bag. As shown in Figure 2D, both the potential and pH cycles were quite reproducible. The pH in the discharged state remained ≈9, as it was initially, and the pH in the charged state

remained ≈12, suggesting the feasibility of cell cycling between pH 9 and 12 when oxygen penetration is eliminated.

The cycling stability of the 2,6-DPPEAQ electrolyte was also studied by the volumetrically unbalanced compositionally symmetric cell method.[11] Although the oxidized form of 2,6-DPPEAQ is readily soluble at pH 9, proton-coupled electron transfer raises the pH of the electrolyte when it is reduced. Such pH oscillations can produce misleading results in symmetric cell testing unless the starting pH is above the cutoff point for proton-coupled electron transfer. The experiment shown in **Figure 3** demonstrates the capacity fade behavior of a compositionally symmetric cell at pH 13, using potentiostatic cycling at ±200 mV to access >99% of the theoretical capacity of the 4.5 mL of 0.1 M limiting electrolyte. The cell was cycled for 6 days at pH 13, exhibiting an average capacity fade rate of 0.02% per day (Figure 3).

High concentration and long-term full cell testing was performed at 20 °C with solutions of 0.5 M of the tetra-potassium salt of 2,6-DPPEAQ in the negolyte and a solution of 0.4 M
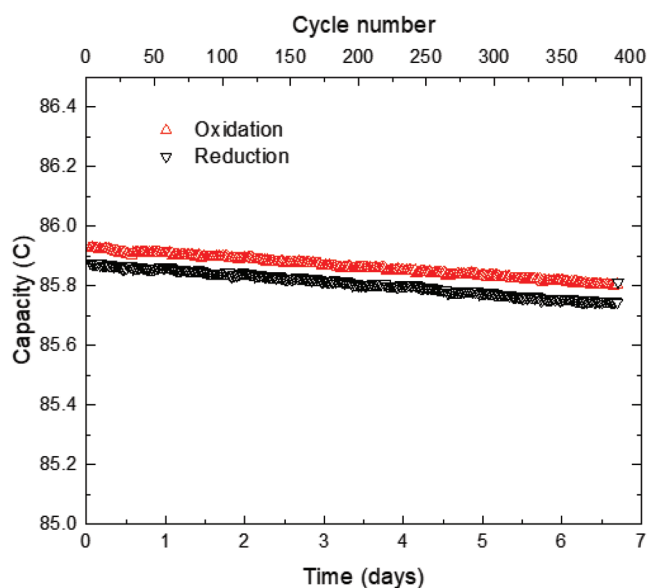
Figure 3. Unbalanced compositionally symmetric cell cycling of 0.1 M of the tetra-potassium salt of 2,6-DPPEAQ at pH 13, showing capacity as a function of time. Capacities were obtained by full potentiostatic reduction and oxidation of the capacity-limiting side at ±0.2 V.

$K_4Fe(CN)_6$ and 0.1 M $K_3Fe(CN)_6$ in the posolyte, both sides dissolved in aqueous solution with pH adjusted to ≈9 by the addition of a trace amount of KOH. The small amount of ferricyanide prevents the posolyte from becoming the capacity-limiting side during discharge in case it undergoes slow reductive side reactions at high state of charge (SOC); this precaution permits us to focus our attention only on the stability of the negolyte. The high solubility and high ionic charge of 2,6-DPPEAQ enable the use of less supporting electrolyte (<10^{-5} M KOH) without compromising the ionic conductivity of the solution. These solutions were pumped through a flow cell constructed from graphite flow plates and carbon paper electrodes, separated by a Fumasep E-620 (K) membrane, which has a low permeability to 2,6-DPPEAQ and ferricyanide as reported in the Supporting Information. The RFB was charged at room temperature, stepwise at constant voltage (1.5 V) with a 10% increment in the quinone (capacity-limiting side) SOC. Polarization curves were measured at 10%, 50%, and 90% SOC. The OCV at 50% SOC is ≈1.02 V. As the SOC increased from 10% to 90%, the OCV increased from 0.95 to 1.05 V (**Figure 4**A). In the galvanic direction, the peak power density was 0.16 W cm^{-2} at 90% SOC (Figure 4B). The area-specific resistance (ASR) of the membrane (1.3 Ω cm^2 at 50% SOC, determined by high-frequency electrochemical impedance spectroscopy (EIS) in the full cell) was responsible for ≈80% of the ASR of the entire cell (1.6 Ω cm^2 at 50% SOC, DC polarization). It is anticipated that a membrane with lower resistivity would raise the power density significantly.

The cell was cycled at a constant current density of ±0.1 A cm^{-2}, and each galvanostatic half-cycle was finished with a potential hold at the potential limit (1.5 V after charge, 0.5 V after discharge) until the magnitude of the current density fell below 2 mA cm^{-2} to avoid temporal variations in accessible capacity during full cell cycling caused by changes in membrane

resistance. The cell, exhibiting 97% of theoretical capacity, was cycled for 480 cycles, which required 12.3 days to complete at 100 mA cm^{-2}. The average capacity retention rate over the 480 cycles was 99.99964% per cycle at an average coulombic efficiency greater than 99.9%, which reflects a capacity fade rate of 0.00036% per cycle or 0.014% per day (Figure 4C). This temporal fade rate is lower than that of any other RFB chemistry reported to date in the absence of rebalancing processes—including our previous record, a ferrocene/viologen-based flow battery with a capacity fade rate of 0.033% per day in full cell testing.[6a] We used galvanostatic cycling with potential holds to relate the capacity fade of the cell to the stability of the limiting electrolyte.[11] Purely galvanostatic cycling cannot be used to assess the cycling stability of an electrolyte because of the confounding effects of changes in the internal resistance of the cell: if the internal resistance drifts upward during long galvanostatic cycling experiments, in later cycles the voltage limits are encountered sooner, causing less of the available capacity to be accessed than in the earlier cycles. The potential holds ensure electrochemical access to the entire SOC range rather than a limited SOC range dictated by ohmic resistance of the cell. Although the galvanostatic portion of the cycling profiles showed a higher capacity fade rate than that of the full galvanostatic+potentiostatic cycles (Figure 4C; Figure S4 and Table S1, Supporting Information), higher average current densities were obtained during the later potentiostatic steps (Figure S5, Supporting Information). This is consistent with the interpretation that an increased internal resistance over long-term cycling caused a higher concentration of reactant species to be left over at the end of the galvanostatic step and accessible during the potentiostatic step.

After 12.3 days of cycling, the pH of the discharged negolyte had increased to nearly 13. Although the cell was run in a glove bag with nitrogen flowing, some atmospheric oxygen apparently penetrated to oxidize the hydroquinone, producing hydroxide. The same experiment was also performed in the glove box, showing the reversible pH oscillations during quinone cell cycling when oxygen is more effectively eliminated (Figure S7, Supporting Information). The sensitivity to reversible chemical oxidation from ambient O_2 exists in any aqueous flow battery whose negolyte redox potential is lower than that of O_2, which is the case for all aqueous flow batteries of which we are aware.[4–9] However, this is not considered to be a significant barrier to the practical implementation of flow batteries, as protection of the negolyte against O_2 has been successfully implemented in commercial-scale all-vanadium flow batteries by purging an inert gas in the reservoir headspace.

Since the recent debut of functionalized quinones in aqueous flow batteries, functionalization efforts have been aimed at raising the solubility, tuning the reduction potential, and extending molecular lifetime.[15] Desirable attributes in these three categories often trade off against each other. The experience gained from studying molecular stability is leading to new, stable molecular structures that retain the initially promising attributes achieved through selective functionalization. We have found that solubilizing groups attached directly to the aryl rings shift the reduction potential most strongly but tend to compromise the molecular lifetime.[4a,9,16] Separating the solubilizing groups from the rings with short alkyl linkages increases the lifetime but limits the shift in reduction potential,
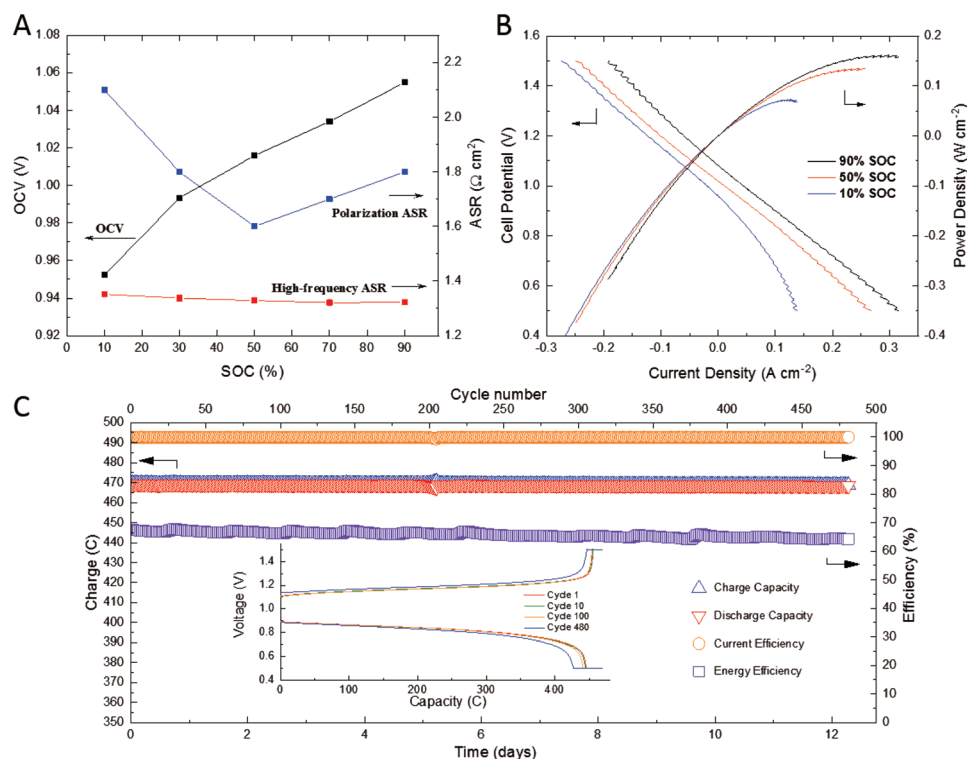
Figure 4. A) Full cell OCV, high-frequency and polarization ASR versus SOC at room temperature at 10, 30, 50, 70, and 90% SOC. Electrolytes comprised 5 mL 0.5 M of the tetra-potassium salt of 2,6-DPPEAQ (negolyte) at pH 9 and 80 mL 0.4 M potassium ferrocyanide and 0.1 M potassium ferricyanide (posolyte) at pH 9. B) Cell potential and power density versus current density. C) CE (circles), energy efficiency (squares), charge (upward-pointing triangles) capacity, and discharge (downward-pointing triangles) capacity versus time and cycle number. The cell was cycled galvanostatically at 100 mA cm^{-2} between 1.5 and 0.5 V, and each half-cycle ended with a potentiostatic hold until the magnitude of the current density fell below 2 mA cm^{-2}. The supply of nitrogen to the glove bag ran out near cycle 202 and was replaced near cycle 211. Inset: capacity versus cell voltage at the 1st, the 10th, the 100th, and the 480th cycle.

typically leading to a lower full-cell OCV. The breakthrough with DBEAQ yielded a cell with multiyear lifetime while maintaining solubility ≥ 1 M electrons and OCV ≥ 1.0 V. The study of DBEAQ degradation led to a phosphonate functionalization in 2,6-DPPEAQ that further enhances the lifetime and solubility while maintaining the OCV ≥ 1.0 V and providing access to less alkaline operating conditions. A 2,6-DPPEAQ full cell at 0.5 M concentration against a ferri/ferrocyanide posolyte exhibited an OCV of 1.0 V, decent power density—especially in light of the inexpensive nonfluorinated polymer membrane employed[9]—and a record-low capacity fade rate (0.00036% per cycle, 0.014% per day, or 5.0% per year). To the best of our knowledge, this is the lowest capacity fade rate in the absence of rebalancing processes ever reported for any RFB chemistry—aqueous or nonaqueous; organic or inorganic; acidic, basic, or neutral pH; monomer, oligomer, or polymer. The economic tradeoff of the present value of small annual replacements of the active species versus the potential capital cost savings from substituting organic for vanadium favors the organic when the interest rate for discounting is high.[5b] If the mass-production cost of 2,6-DPPEAQ turns out to be nearly as low as for other substituted anthraquinones that have been studied,[5b,9,17] then this chemistry is the most promising candidate developed thus far for grid scale energy storage.

Supporting Information

Supporting Information is available from the Wiley Online Library or from the author.

Acknowledgements

Conflict of Interest

The authors declare no conflict of interest.

[1] a) B. Dunn, H. Kamath, J.-M. Tarascon, *Science* **2011**, *334*, 928; b) Z. Yang, J. Zhang, M. C. W. Kintner-Meyer, X. Lu, D. Choi, J. P. Lemmon, J. Liu, *Chem. Rev.* **2011**, *111*, 3577; c) B. Obama, *Science* **2017**, *355*, 126.

[2] a) T. Nguyen, R. F. Savinell, *Electrochem. Soc. Interface* **2010**, *19*, 54; b) M. Skyllas-Kazacos, M. H. Chakrabarti, S. A. Hajimolana, F. S. Mjalli, M. Saleem, *J. Electrochem. Soc.* **2011**, *158*, R55; c) W. Liu, W. Lu, H. Zhang, X. Li, *Chem. - Eur. J.* **2018**, *24*, 9525; d) C. Zhang, L. Zhang, Y. Ding, S. Peng, X. Guo, Y. Zhao, G. He, G. Yu, *Energy Storage Mater.* **2018**, *15*, 324; e) K. Gong, Q. Fang, S. Gu, S. F. Y. Li, Y. Yan, *Energy Environ. Sci.* **2015**, *8*, 3515.

[3] a) G. L. Soloveichik, *Chem. Rev.* **2015**, *115*, 11533; b) J. Winsberg, T. Hagemann, T. Janoschka, M. D. Hager, U. S. Schubert, *Angew. Chem., Int. Ed.* **2017**, *56*, 686.

[4] a) B. Huskinson, M. P. Marshak, C. Suh, S. Er, M. R. Gerhardt, C. J. Galvin, X. Chen, A. Aspuru-Guzik, R. G. Gordon, M. J. Aziz, *Nature* **2014**, *505*, 195; b) T. Janoschka, N. Martin, U. Martin, C. Friebe, S. Morgenstern, H. Hiller, M. D. Hager, U. S. Schubert, *Nature* **2015**, *527*, 78; c) K. Lin, Q. Chen, M. R. Gerhardt, L. Tong, S. B. Kim, L. Eisenach, A. W. Valle, D. Hardee, R. G. Gordon, M. J. Aziz, M. P. Marshak, *Science* **2015**, *349*, 1529; d) K. Lin, R. Gómez-Bombarelli, E. S. Beh, L. Tong, Q. Chen, A. Valle, A. Aspuru-Guzik, M. J. Aziz, R. G. Gordon, *Nat. Energy* **2016**, *1*, 16102; e) B. Yang, L. Hoober-Burkhardt, S. Krishnamoorthy, A. Murali, G. K. S. Prakash, S. R. Narayanan, *J. Electrochem. Soc.* **2016**, *163*, A1442; f) A. Orita, M. G. Verde, M. Sakai, Y. S. Meng, *Nat. Commun.* **2016**, *7*, 13230; g) X. Wei, W. Xu, J. Huang, L. Zhang, E. Walter, C. Lawrence, M. Vijayakumar, W. A. Henderson, T. Liu, L. Cosimbescu, B. Li, V. Sprenkle, W. Wang, *Angew. Chem., Int. Ed.* **2015**, *54*, 8684; h) Y. Ding, Y. Li, G. Yu, *Chem* **2016**, *1*, 790; i) J. D. Milshtein, A. P. Kaur, M. D. Casselman, J. A. Kowalski, S. Modekrutti, P. L. Zhang, N. Harsha Attanayake, C. F. Elliott, S. R. Parkin, C. Risko, F. R. Brushett, S. A. Odom, *Energy Environ. Sci.* **2016**, *9*, 3531; j) C. S. Sevov, D. P. Hickey, M. E. Cook, S. G. Robinson, S. Barnett, S. D. Minteer, M. S. Sigman, M. S. Sanford, *J. Am. Chem. Soc.* **2017**, *139*, 2924; k) B. Hu, T. L. Liu, *J. Energy Chem.* **2018**, *27*, 1326.

[5] a) B. Yang, L. Hoober-Burkhardt, F. Wang, G. K. Surya Prakash, S. R. Narayanan, *J. Electrochem. Soc.* **2014**, *161*, A1371; b) Z. Yang, L. Tong, D. P. Tabor, E. S. Beh, M. A. Goulet, D. Porcellinis, A. Aspuru-Guzik, R. G. Gordon, M. J. Aziz, *Adv. Energy Mater.* **2018**, *8*, 1702056.

[6] a) E. S. Beh, D. De Porcellinis, R. L. Gracia, K. T. Xia, R. G. Gordon, M. J. Aziz, *ACS Energy Lett.* **2017**, *2*, 639; b) C. DeBruler, B. Hu, J. Moss, J. Luo, T. L. Liu, *ACS Energy Lett.* **2018**, *3*, 663; c) B. Hu, C. DeBruler, Z. Rhodes, T. L. Liu, *J. Am. Chem. Soc.* **2017**, *139*, 1207; d) C. DeBruler, B. Hu, J. Moss, X. Liu, J. Luo, Y. Sun, T. L. Liu, *Chem* **2017**, *3*, 961; e) T. Janoschka, S. Morgenstern, H. Hiller, C. Friebe, K. Wolkersdorfer, B. Hauptler, M. D. Hager, U. S. Schubert, *Polym. Chem.* **2015**, *6*, 7801; f) T. Liu, X. Wei, Z. Nie, V. Sprenkle, W. Wang, *Adv. Energy Mater.* **2016**, *6*, 1501449.

[7] a) J. Winsberg, C. Stolze, A. Schwenke, S. Muench, M. D. Hager, U. S. Schubert, *ACS Energy Lett.* **2017**, *2*, 411; b) J. Winsberg, T. Janoschka, S. Morgenstern, T. Hagemann, S. Muench, G. Hauffman, J. F. Gohy, M. D. Hager, U. S. Schubert, *Adv. Mater.* **2016**, *28*, 2238; c) J. Winsberg, C. Stolze, S. Muench, F. Liedl, M. D. Hager, U. S. Schubert, *ACS Energy Lett.* **2016**, *1*, 976.

[8] A. Hollas, X. Wei, V. Murugesan, Z. Nie, B. Li, D. Reed, J. Liu, V. Sprenkle, W. Wang, *Nat. Energy* **2018**, *3*, 508.

[9] D. G. Kwabi, K. Lin, Y. Ji, E. F. Kerr, M.-A. Goulet, D. De Porcellinis, D. P. Tabor, D. A. Pollack, A. Aspuru-Guzik, R. G. Gordon, M. J. Aziz, *Joule* **2018**, *2*, 1894.

[10] DPPEAQ is an abbreviation for a di-(3-phosphonic acid)propyl ether of anthraquinone.

[11] M.-A. Goulet, M. J. Aziz, *J. Electrochem. Soc.* **2018**, *165*, A1466.

[12] M. B. Smith, *March's Advanced Organic Chemistry: Reactions, Mechanisms and Structure*, 7th ed., Wiley, NY **2013**.

[13] M. Quan, D. Sanchez, M. F. Wasylkiw, D. K. Smith, *J. Am. Chem. Soc.* **2007**, *129*, 12847.

[14] a) J. Luo, A. Sam, B. Hu, C. DeBruler, X. Wei, W. Wang, T. L. Liu, *Nano Energy* **2017**, *42*, 215; b) S. Y. Reece, *US patent application US20160149251A1*, **2016**.

[15] K. Wedege, E. Dražević, D. Konya, A. Bentien, *Sci. Rep.* **2016**, *6*, 39101.

[16] a) M. R. Gerhardt, L. Tong, R. Gómez-Bombarelli, Q. Chen, M. P. Marshak, C. J. Galvin, A. Aspuru-Guzik, R. G. Gordon, M. J. Aziz, *Adv. Energy Mater.* **2017**, *7*, 1601488; b) M. R. Gerhardt, E. S. Beh, L. Tong, R. G. Gordon, M. J. Aziz, *MRS Adv.* **2017**, *2*, 431.

[17] V. Dieterich, J. Milshtein, J. Barton, T. Carney, R. Darling, F. Brushett, *Transl. Mater. Res.* **2018**, *5*, 034001.

ADVANCED ENERGY MATERIALS

Supporting Information

A Phosphonate-Functionalized Quinone Redox Flow Battery at Near-Neutral pH with Record Capacity Retention Rate

Yunlong Ji, Marc-Antoni Goulet, Daniel A. Pollack, David G. Kwabi, Shijian Jin, DianaDe Porcellinis, Emily F. Kerr, Roy G. Gordon,* and Michael J. Aziz*

Supporting Information

A phosphonate-functionalized quinone redox flow battery at near-neutral pH

with record capacity retention rate

Yunlong Ji, Marc-Antoni Goulet, Daniel A. Pollack, David G. Kwabi, Shijian Jin, Diana De Porcellinis, Emily F. Kerr, Roy G. Gordon* and Michael J. Aziz*

Dr. Yunlong Ji, Emily F. Kerr, Prof. Roy G. Gordon
Department of Chemistry and Chemical Biology, Harvard University, 12 Oxford Street, Cambridge, Massachusetts 02138, USA
Email: gordon@chemistry.harvard.edu

Dr. Marc-Antoni Goulet, Dr. David G. Kwabi, Shijian Jin, Dr. Diana De Porcellinis, Prof. Roy G Gordon, Prof. Michael J Aziz
Harvard John A. Paulson School of Engineering and Applied Sciences, 29 Oxford Street, Cambridge, Massachusetts 02138, USA
Email: maziz@harvard.edu

Daniel A. Pollack
Department of Physics, Harvard University, 17 Oxford St, Cambridge, Massachusetts 02138, USA

*Corresponding authors:

Roy G. Gordon
Cabot Professor
Department of Chemistry and Chemical Biology
12 Oxford Street, MA 02138, USA
Tel: +1 617-495-4017
Fax: +1 617-495-4723
email: Gordon@chemistry.harvard.edu

Michael J. Aziz
Gene and Tracy Sykes Professor of Materials and Energy Technologies
Harvard John A. Paulson School of Engineering and Applied Sciences, Pierce Hall 204a
29 Oxford Street, MA 02138, USA
Tel: +1 (617) 495-9884
email: maziz@harvard.edu

Contents

Synthesis and Chemical Characterization

Synthesis of (((9,10-dioxo-9,10-dihydroanthracene-2,6-diyl)bis(oxy))bis(propane-3,1-diyl))bis(phosphonic acid):

2,6-dihydroxyanthraquinone (2,6-DHAQ) was purchased from AK Scientific. All other chemicals were purchased from Sigma Aldrich. All chemicals were used as received unless specified otherwise.
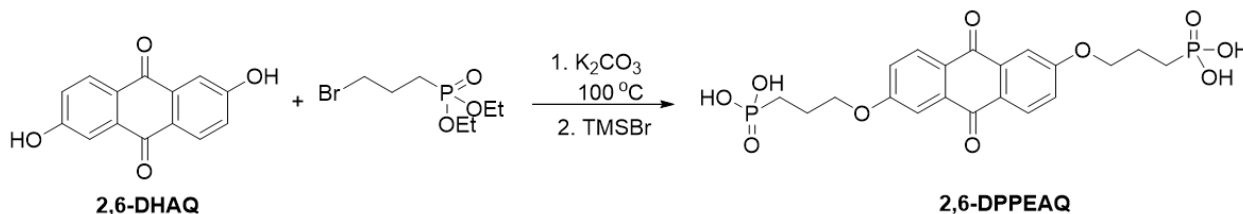
Scheme S1. Synthesis of **2,6-DPPEAQ**.

(((9,10-dioxo-9,10-dihydroanthracene-2,6-diyl)bis(oxy))bis(propane-3,1 diyl))bis(phosphonic acid):

2,6-DHAQ (10 mmol) was mixed with anhydrous K$_2$CO$_3$ (40 mmol) and diethyl (3-bromopropyl)phosphonate (30 mmol) in DMF (50 mL). The reaction mixture was then heated to 100 °C overnight. After removing the solvent, the solid was washed thoroughly with DI water. The product was analyzed by ^{1}H NMR and used for the next reaction step without further purification.

The ester precursor of 2,6-DPPEAQ was dissolved in dichloromethane (100 mL), and trimethylsilyl bromide (100.0 mmol) was added. After 15 h stirring at room temperature, the solvent and excess TMSBr were distilled off. The mixture was washed thoroughly with DI water and hexane, then vacuum dried to yield yellow solid. Final yield: 98%. ^{1}H NMR (500 MHz, DMSO-d$_6$) δ 8.13 (d, J = 8.6 Hz, 2H), 7.56 (d, J = 2.7 Hz, 2H), 7.40 (dd, J = 8.7, 2.7 Hz, 2H), 4.24 (t, J = 6.4 Hz, 4H), 1.96 (m, 4H), 1.69 (m, 4H).
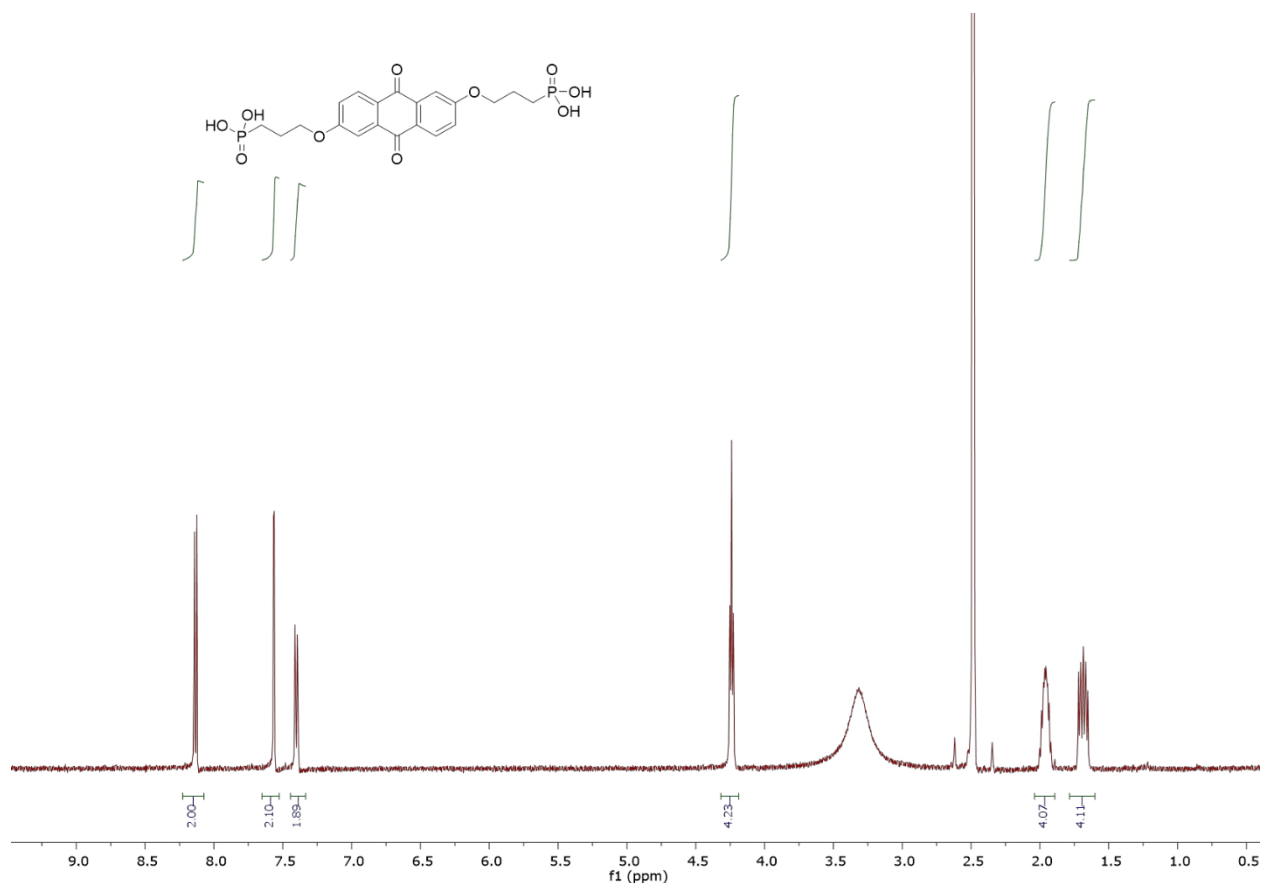

Figure S1. ^{1}H NMR spectrum of 2,6-DPPEAQ. Solvent peaks are those that are not integrated.

Electrochemical Characterization

Cyclic Voltammetry (CV) and Rotating Disk Electrode (RDE) Measurements

Glassy carbon was used as the working electrode for all three-electrode CV tests. RDE experiments were conducted using a Pine Instruments Modulated Speed Rotator AFMSRCE equipped with a 5 mm diameter glassy carbon working electrode, a Ag/AgCl reference electrode (BASi, pre-soaked in a 3 M KCl solution), and a graphite counter electrode. The diffusion coefficient of the oxidized form of 2,6-DPPEAQ was calculated using the Levich equation, which relates the mass-transport-limited current to the number of electrons transferred (n), the area of the electrode (A), and the concentration of redox-active species in the electrolyte (C) by plotting the mass-transport-limited current against the square root of the rotation rate (**Figure S2**) with the following parameters: n = 2, F = 96,485 Coulombs/mol, A = 0.196 cm^2, C = 5 mM, kinematic viscosity of 1 M KOH ν = 1.08 × 10^{-6} m^2/s. The resulting value of the diffusion coefficient for the oxidized form of 2,6-DPPEAQ is 1.37 × 10^{-6} cm^2/s.
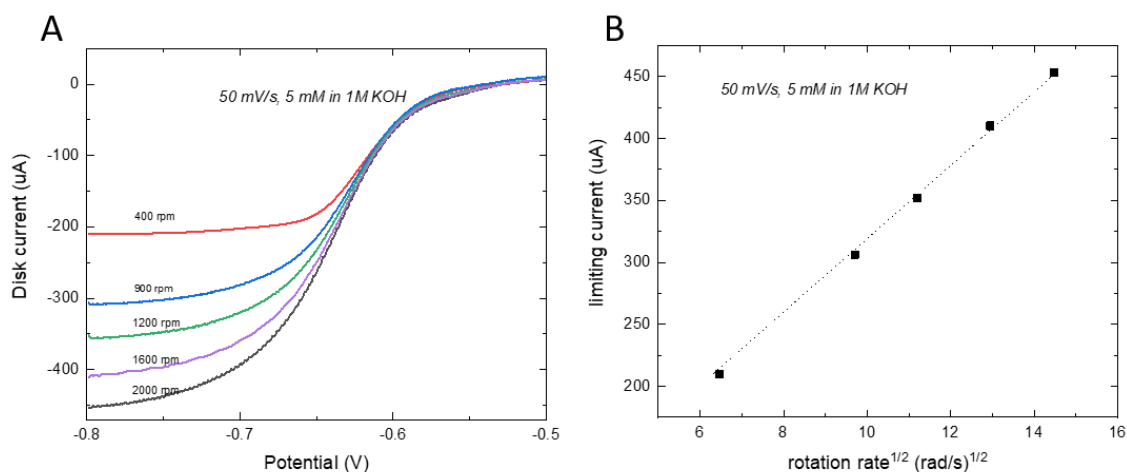

Figure S2. (A) Rotating Disk Electrode study of the reduction of 5 mM 2,6-DPPEAQ in 1M KOH on a glassy carbon electrode at rotation rates between 400 and 2000 rpm. (B) Levich plot (limiting current vs square root of rotation rate in rad/s) of 5 mM 2,6-DPPEAQ in 1 M KOH. Limiting current is taken as the current at -0.8 V in (A). The slope yields a diffusion coefficient for the oxidized form of 2,6-DPPEAQ of 1.37 × 10^{-6} cm^2 s^{-1}.
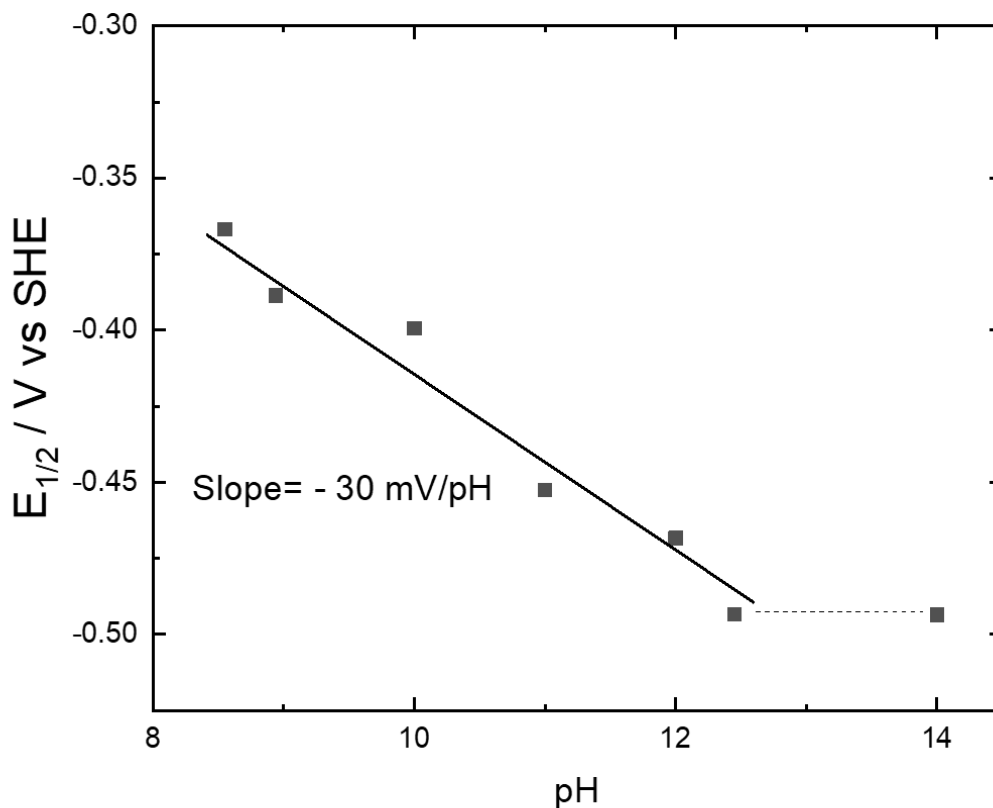
Figure S3. Pourbaix diagram of 2,6-DPPEAQ with a slope of -30 mV/pH fit to the data below pH 12. All of the potentials were determined by cyclic voltammograms of 1 mM 2,6-DPPEAQ in buffered solutions. Above pH ~ 12.4, the potential is pH-independent, indicating that both oxidized and reduced forms of 2,6-DPPEAQ are deprotonated. The dashed line has zero slope.

Symmetric and Full Cell Measurements

Flow battery experiments were conducted with cell hardware from Fuel Cell Tech. (Albuquerque, NM), assembled into a zero-gap flow cell configuration, similar to a previous report.[1] Pyrosealed POCO graphite flow plates with serpentine flow patterns were used for both electrodes. Each electrode comprised a 5 cm^2 geometric surface area covered by a stack of three or four sheets of Sigracet SGL 39AA porous carbon paper pre-baked in air for 8 h at 400°C.

For symmetric cell tests, a sheet of Nafion 117 membrane soaked for 8 h in 1 M KOH served as the ion-selective membrane between the carbon electrodes, whereas for full cell tests, a Fumasep E-620 (K) membrane was used. The outer portion of the space between the electrodes was gasketed by Viton sheets with the area over the electrodes cut out. Torque applied during cell assembly was 60 lb-in on each of 8 bolts. The electrolytes were fed into the cell through fluorinated ethylene propylene (FEP) tubing at a rate of 60 mL/min, controlled by Cole-Parmer

Masterflex L/S peristaltic pumps. All cells were run inside a nitrogen-filled glove box with an O_2 partial pressure of about 1 to 2 ppm. Cell polarization measurements, impedance spectroscopy, and charge-discharge cycling were performed using a Biologic VSP 300 potentiostat.

Full cell cycling (i.e., with a ferro/ferricyanide-based posolyte) was performed with the same flow cell hardware but with a Fumasep E-620 (K) membrane due to its low permeability of 2,6-DPPEAQ and ferricyanide. Galvanostatic cycling was performed at ±0.1 A cm^{-2} at room temperature, with voltage limits of 0.5 and 1.5 V. To obtain the polarization curves, the cell was first charged to the desired state of charge and then polarized via linear sweep voltammetry at a rate of 100 mV s^{-1}. This method was found to yield polarization curves very close to point-by-point galvanostatic holds, yet to impose minimal perturbation to the SOC of the small-electrolyte-volume cell. Electrochemical impedance spectroscopy (EIS) was performed at SOCs between 10 and 100% at open-circuit potential with a 10 mV perturbation and with frequency ranging from 1 to 300,000 Hz.
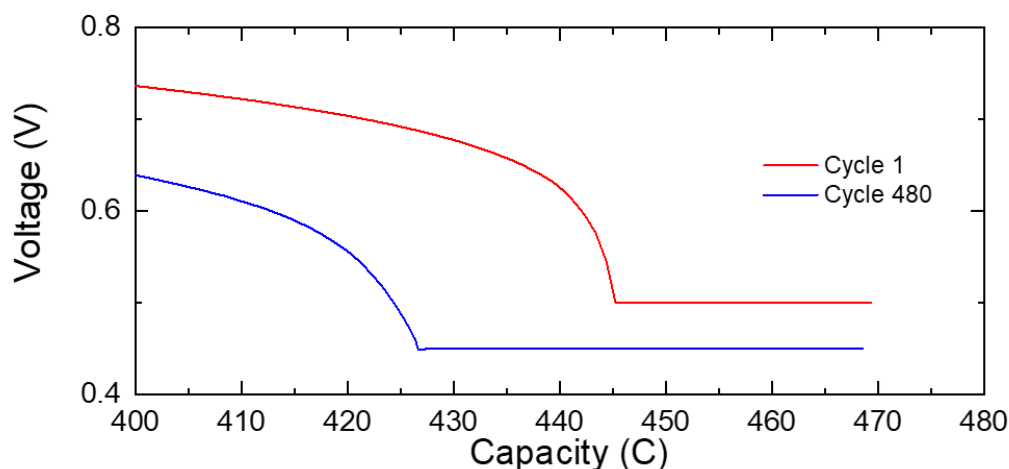

Figure S4. Magnification of the potentiostatic regions of the first and last discharge cycle in Figure 4C inset, offset vertically for clarity.
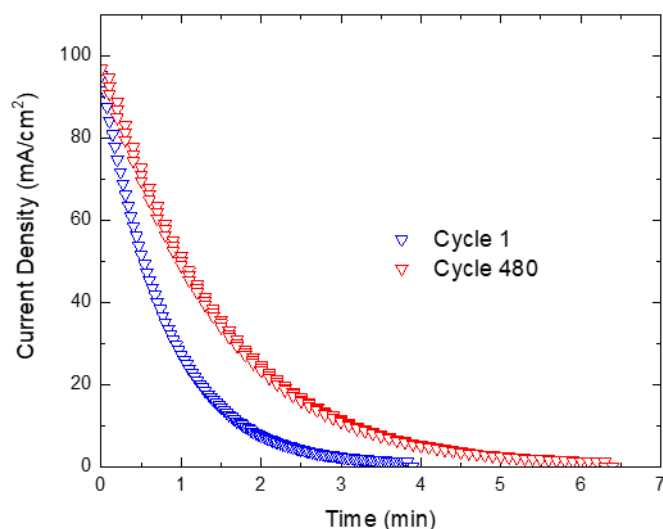
Figure S5. Current density vs time in the potentiostatic step of the first and last discharge cycle from the cell in Figure 4.

Table S1. Capacity and time of galvanostatic step and potentiostatic step of the first and last discharge cycle from the cell in Figure 4.

Cycle	Capacity (C)		Time (min)	
	galvanostatic	potentiostatic	galvanostatic	potentiostatic
1	445.24	24.13	14.9	4.0
480	426.69	41.86	14.0	6.0

Table S2. Conductivity and viscosity of the electrolytes from the cell in Figure 4.

Electrolyte	Negolyte	Posolyte
Conductivity (mS/cm)	67.7 ± 1.8	147.7 ± 1.5
Viscosity (centipoise)	3.047 ± 4.7%	2.553 ± 2.6%

before-cycling

2

Before Cycling

after-cycling

1

After Cycling

9.5   9.0   8.5   8.0   7.5   7.0   6.5   6.0   5.5   5.0   4.5   4.0   3.5   3.0   2.5   2.0   1.5   1.0   0.5   0.0
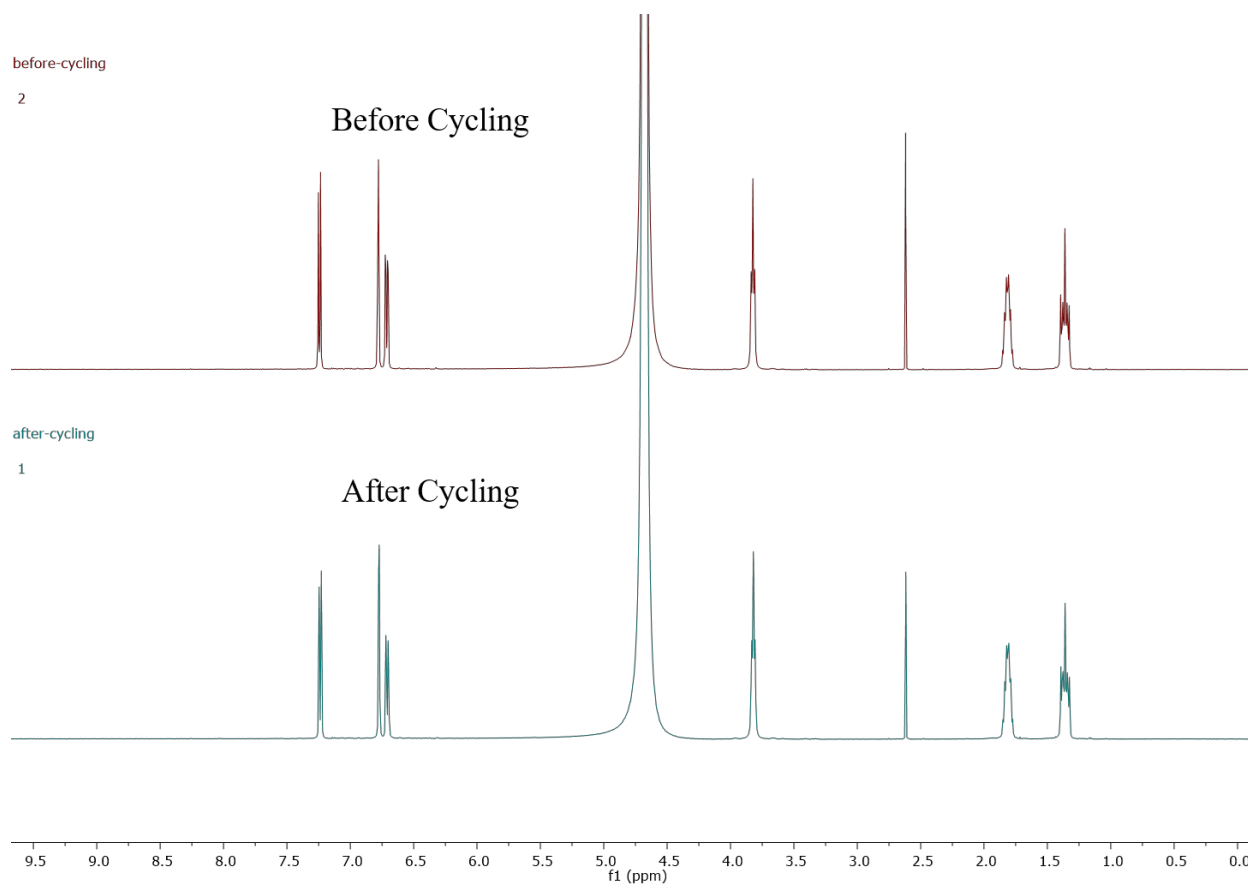f1 (ppm)

Figure S6. ^{1}H NMR spectra (500 MHz) of negolyte before (top) and after (bottom) cycling from the cell in Figure 4.

No evidence of 2,6-DPPEAQ decomposition was observed in the cycled electrolytes. The NMR in **Figure S6** is taken from the full cell cycling experiment in **Figure 4**. New impurity peaks were not detected. However, as the detection limit for NMR is ~1%, at a capacity fade rate of 0.014%/day, it will take at least 70 days of cycling to be able to detect any decomposition products. The sensitivity of CV is lower still. Furthermore, species crossover was not detected by NMR, CV, or UV-Vis spectrophotometry; this is no surprise given the minuscule amount of capacity fade observed.
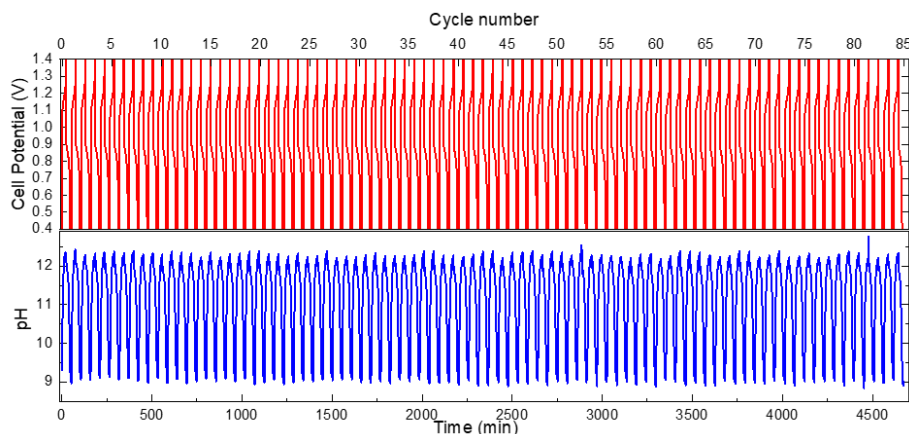
Figure S7. Representative curves of cell potential and negolyte pH vs time of the 2,6-DPPEAQ cell in the glove box. Electrolytes comprised 5 mL 0.5 M 2,6-DPPEAQ (negolyte) at pH 9 and 80 mL 0.4 M potassium ferrocyanide and 0.1 M potassium ferricyanide (posolyte) at pH 9. The pH probe was immersed in the negolyte to monitor the pH of the solution.

Volumetric Capacity and Energy Density

Based on solubility limits, the negative electrolyte of 0.75 M 2,6-DPPEAQ, with two electrons per molecule, has a theoretical volumetric capacity of 40.2 Ah/L. The positive electrolyte of 1.2 M ferrocyanide[2], has a theoretical volumetric capacity of 32.2 Ah/L. Thus, the energy density of the battery is limited by the positive side, with a theoretical energy density of 17.9 Wh/L. However, using established methods of raising the ferrocyanide solubility to 1.5 M[3], the energy density would become 20.1 Wh/L.

In the experimental cell in **Figure 4**, the negative electrolyte of 0.5 M 2,6-DPPEAQ has a demonstrated volumetric capacity of 26.8 Ah/L. The positive electrolyte of 0.4 M ferrocyanide has a demonstrated volumetric capacity of 10.7 Ah/L. The demonstrated energy density is 7.7 Wh/L.

Chemical Stability Experiments

Samples of 2,6-DPPEAQ at 0.1 M concentration and at pH 9, 12, and 14 (two equivalent samples each) were stored in FEP bottles (VWR Catalog No. 16071-008) and heated in an oven at 95 °C for 6 days. The extent of decomposition was determined by ^{1}H NMR, with peak integrals measured relative to an internal standard of $NaCH_3SO_3$ prepared at 10 mM concentration in D_2O. All samples were diluted in this deuterated solvent containing the internal standard at a fixed ratio of 1:5.

A 2,6-DPPEAQ at pH 14

B 2,6-DPPEAQ at pH 14, treated 5.5 days at 95 °C and 0.1 M

C 2,6-DBEAQ at pH 14

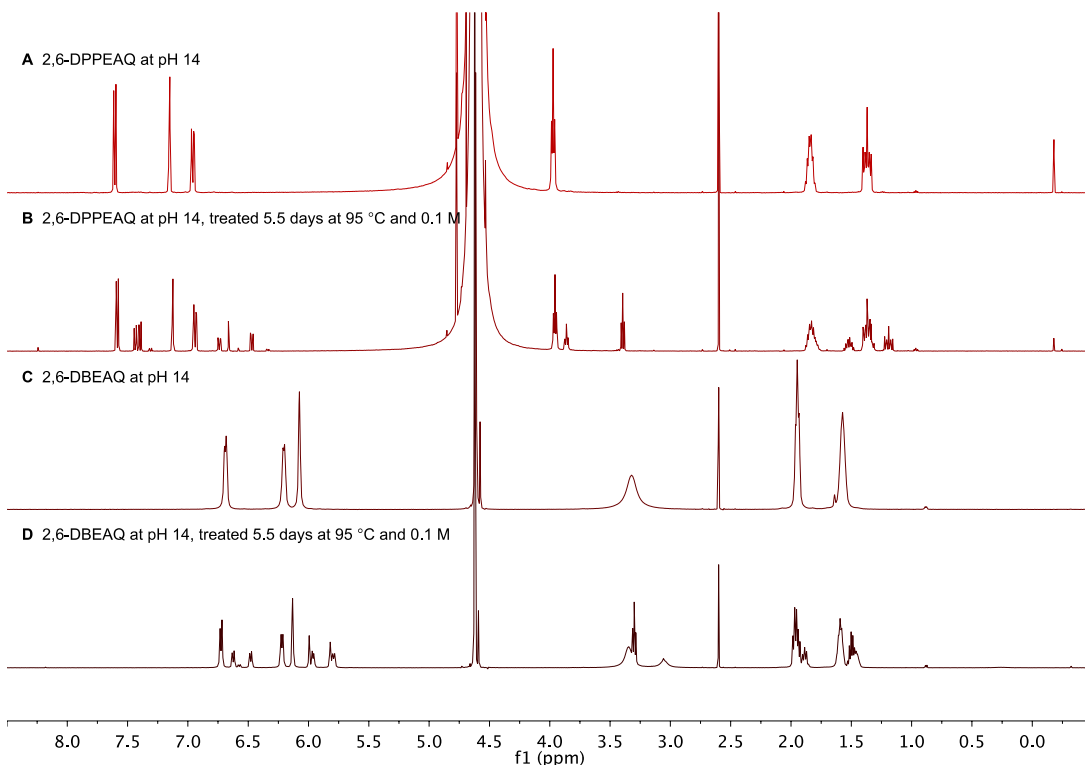D 2,6-DBEAQ at pH 14, treated 5.5 days at 95 °C and 0.1 M

Figure S8. Comparison of the stability of 2,6-DPPEAQ with respect to alkyl chain cleavage to that of 2,6-DBEAQ at pH 14, all at 0.1 M quinone concentration in aqueous solution. ^{1}H NMR spectra (500 MHz, 10 mM NaCH$_3$SO$_3$ internal standard, δ 2.6 ppm) of 2,6-DPPEAQ at pH 14, (A) before and (B) after treatment for 5.5 days at 95 °C; 2,6-DBEAQ at pH 14, (C) before and (D) after treatment for 5.5 days at 95 °C. After 95 °C treatment, 2,6-DBEAQ and 2,6-DPPEAQ both exhibit 45% decomposition. The relative integrals and splittings of the peaks in the spectra of 2,6-DPPEAQ after treatment are consistent with the products of (3-hydroxypropyl)phosphonate cleavage.

Additionally, samples of 2,6-DPPEAQ at 0.1 M concentration and pH 14 in both the oxidized and reduced form were stored in FEP bottles and heated in an oven at 65 °C for 2 weeks. The extent of decomposition was determined by ^{1}H NMR, with peak integrals measured relative to an internal standard of NaCH$_3$SO$_3$ prepared at 10 mM concentration in D$_2$O.
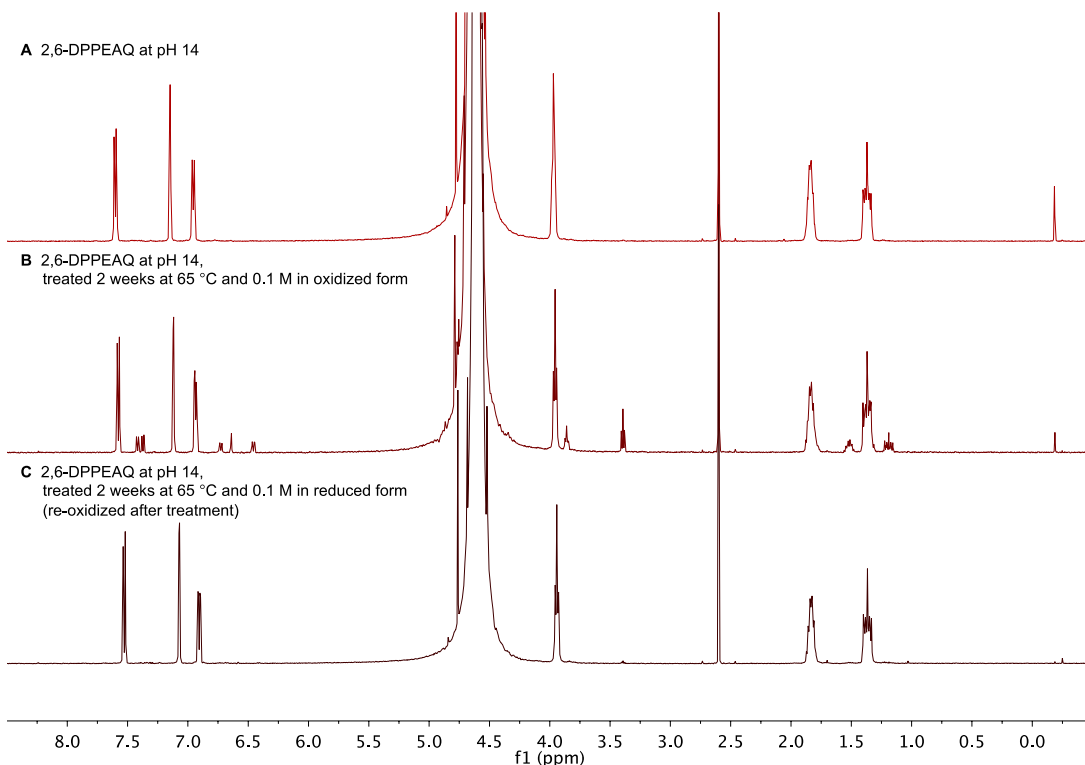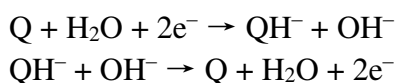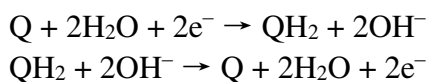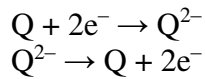
Figure S9. Comparison of 2,6-DPPEAQ stability in the oxidized and reduced forms at pH 14 and at 0.1 M concentration in aqueous solution. ^{1}H NMR spectra (500 MHz, 10 mM NaCH$_3$SO$_3$ internal standard, δ 2.6 ppm) of (A) 2,6-DPPEAQ at pH 14; (B) 2,6-DPPEAQ at pH 14, treated for 2 weeks at 65 °C in the oxidized form; (C) 2,6-DPPEAQ at pH 14, treated for 12 days at 65 °C in the reduced form (sample re-oxidized prior to collecting ^{1}H NMR spectrum). Unlike the oxidized form of 2,6-DPPEAQ, the reduced form exhibits robust chemical stability after treatment, even at pH 14.

Effects of Oxygen and Cell Cycling on Negolyte pH

Effect of Hydroquinone Autoxidation on Negolyte pH

The increase in pH due to quinone reduction is reversible if hydroquinone is oxidized electrochemically. The net equations for the electrochemical reduction of quinones and oxidation of hydroquinones in the three possible hydroquinone protonation states (designated by QH$_2$, QH$^-$, and Q^{2-} depending on the protonation state of the hydroquinone phenol groups) are:

$$Q + 2H_2O + 2e^- \rightarrow QH_2 + 2OH^-$$
$$QH_2 + 2OH^- \rightarrow Q + 2H_2O + 2e^-$$

$$Q + H_2O + 2e^- \rightarrow QH^- + OH^-$$
$$QH^- + OH^- \rightarrow Q + H_2O + 2e^-$$

11

$$Q + 2e^- \rightarrow Q^{2-}$$
$$Q^{2-} \rightarrow Q + 2e^-$$

If, however, the hydroquinones are oxidized by molecular oxygen, then the increase in pH due to quinone reduction is irreversible. Quinone is instead acting as a mediator for the oxygen reduction reaction (ORR), coupled to the oxidation of the species against which the quinones were charged:

$$Q + 2H_2O + 2e^- \rightarrow QH_2 + 2OH^-$$
$$QH_2 + \tfrac{1}{2}\,O_2 \rightarrow Q + H_2O$$
$$\overline{H_2O + \tfrac{1}{2}\,O_2 + 2e^- \rightarrow 2OH^-} \qquad (ORR)$$

$$Q + H_2O + 2e^- \rightarrow QH^- + OH^-$$
$$QH^- + \tfrac{1}{2}\,O_2 \rightarrow Q + OH^-$$
$$\overline{H_2O + \tfrac{1}{2}\,O_2 + 2e^- \rightarrow 2OH^-} \qquad (ORR)$$

$$Q + 2e^- \rightarrow Q^{2-}$$
$$Q^{2-} + H_2O + \tfrac{1}{2}\,O_2 \rightarrow Q + 2OH^-$$
$$\overline{H_2O + \tfrac{1}{2}\,O_2 + 2e^- \rightarrow 2OH^-} \qquad (ORR)$$
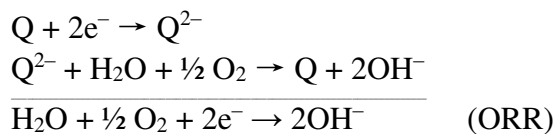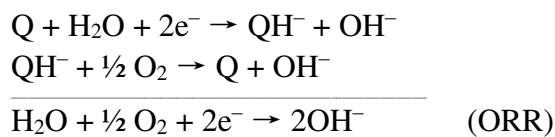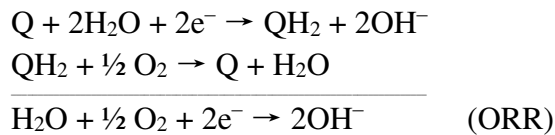
The net result of these reactions with molecular oxygen is therefore an irreversible increase in pH.

Note that if hydrogen peroxide is an intermediate via the reduction of molecular oxygen to peroxide (the autoxidation of anthrahydroquinones is commonly employed in the industrial synthesis of hydrogen peroxide),[4] the net reaction remains the same as above after accounting for the disproportionation reaction of hydrogen peroxide to molecular oxygen and water.

Prediction of Negolyte pH in Charged State

The pH of the negolyte when fully charged is given by the implicit equation:

$$\mathrm{pH} = \log\left[10^{\mathrm{pH}_0 - 14} + \frac{[Q]}{1 + 10^{\mathrm{pH} - \mathrm{pK_a}}}\right] + 14$$

,

where $\mathrm{pK_a}$ is the hydroquinone $\mathrm{pK_{a2}}$ ($\mathrm{pK_{a1}}$ is neglected here for simplicity); $[Q] \equiv [Q^{2-}] + [QH^-]$ is the total hydroquinone concentration (all quinone is in the hydroquinone form when fully charged); and pH_0 is the pH of the negolyte when fully discharged. pH_0 includes contributions from the initial pH before cycling and any irreversible pH increase due to hydroquinone autoxidation.

By solving the above implicit equation with $pH_0 = 9$ and $[Q] = 0.1$ M, the pH of the negolyte in the fully charged state is calculated to be 12.2 when the hydroquinone pK_{a2} is set to 11.5. Even when the pH in the discharged state is increased to 10.5, the above equation predicts that the pH in the charged state will remain at 12.2.

The equation is derived from the Henderson-Hasselbalch equation[5] for the Q^{2-} / QH^- acid-base equilibrium, combined with the constraint that the total hydroquinone concentration $[Q] \equiv [Q^{2-}]$ + $[QH^-]$ (the concentration of the fully protonated hydroquinone $[QH_2]$ is neglected here for simplicity as it is dramatically suppressed near pH 12, but it is included in a more exact calculation described below, which gives nearly identical results). Because each singly protonated hydroquinone QH^- abstracts a proton from the aqueous solution, each contributes a single hydroxide ion to solution. Therefore, the concentration of hydroxide ions in the fully charged state is equal to the initial contribution of 10^{pH_0-14} M from the pH of the discharged state plus the concentration of the singly deprotonated hydroquinone $[QH^-]$. The hydroxide ion concentration is related to the pH by the water-dissociation constant, $K_w = 10^{-14}$.

A similar analysis in which pK_{a1} is retained and $[Q] \equiv [Q^{2-}]$ + $[QH^-]$ + $[QH_2]$ affords the following more exact equation:

$$pH = \log \left[10^{pH_0-14} + \frac{\left(2 + 10^{pH-pK_{a1}}\right) [Q]}{1 + 10^{pH-pK_{a1}} \left(1 + 10^{pH-pK_{a2}}\right)} \right] + 14$$

Solutions to this equation using the values described above are nearly identical, even with pK_{a1} set as high as pK_{a2}.

Permeability Measurements

The permeability of the electroactive molecules was measured in a lab-made two compartment diffusion cell. A 0.1 M solution of the tetra-potassium salt of 2,6-DPPEAQ in KOH at pH 14 was placed on the donating side and paired with 0.2 M KCl in pH 14 KOH on the receiving side to osmotically balance the two sides. To keep the solutions under agitation, the cell was placed on a nutating table. The increase of 2,6-DPPEAQ concentration in the receiving side was measured as a function of time with UV-visible absorption spectrophotometry (Ocean Optics Flame-S Spectrometer Assembly). For each time point, a 400 µL aliquot of the solution on the receiving side was taken and diluted, its concentration was measured by UV-visible spectrophotometry, and it was replaced by fresh 0.2 M KCl solution.

Due to a very low crossover rate and to the detection limit of the spectrometer, we were only able to estimate a maximum value of 2,6-DPPEAQ permeability. According to the derivation of Fick's Law as reported previously,[2] 2,6-DPPEAQ permeability must be lower than 3.4×10^{-13} cm^2/s. Ferricyanide permeability has been measured and published previously for this membrane and is equal to 4.4×10^{-12} cm^2/s.[2]

Solubility Tests

The solubility limit of 2,6-DPPEAQ was measured in the oxidized form by adding the potassium salt of 2,6-DPPEAQ (prepared by reacting 2,6-DPPEAQ with potassium hydroxide in water) until no further solid could be dissolved. The mixture was adjusted to pH 9. After filtering the mixture through a PTFE 0.45 μm syringe filter, a saturated solution of 2,6-DPPEAQ at pH 9 was obtained. The saturated solution was then diluted by a known amount while maintaining a pH of 9, and the concentration was evaluated by UV-visible spectrophotometry (Agilent Cary 60 spectrophotometer). The concentration was calculated according to a pre-calibrated absorbance-concentration curve of known concentrations of 2,6-DPPEAQ at pH 9. The resulting value of the solubility of the oxidized form of 2,6-DPPEAQ at pH 9 is 0.75 M.

The solubility of the oxygen-sensitive reduced form of 2,6-DPPEAQ was not measured but was assumed to be higher than the oxidized form because: (1) no precipitation after full electrochemical reduction of 2,6-DPPEAQ was observed, and (2) the increased negative charges of 2,6-DPPEAQ in the reduced form compared to 2,6-DPPEAQ in the oxidized form is expected to render quinone-quinone interactions even more unfavorable and increase its solubility.

Table S3. Physicochemical properties and performance metrics of three different AQ molecules.

Negolyte	2,6-DHAQ[1, 6]	2,6-DBEAQ[2]	2,6-DPPEAQ
Solubility (M)	0.6 [a]	1.1 [a] (0.6 [b])	0.75 [c]
Diffusion coefficient ($cm^2 s^{-1}$)	4.8×10^{-6}	1.58×10^{-6}	1.37×10^{-6}
Symmetric cell Fading rate (%/day)	5 [d]	0.0080 [d] (0.0075 [e])	0.02 [f]
Full cell Fading rate (%/day)	7.6 [g]	0.04 [h]	0.014 [i]

[a] at pH 14; [b] at pH 12; [c] at pH 9; [d] 0.1 M at pH 14; [e] 0.65 M at pH 14; [f] 0.1 M at pH 13; [g] 0.5 M at pH 14; [h] 0.5 M at pH 12; [i] 0.5 M at pH 9.

References

[1]   K. Lin, Q. Chen, M. R. Gerhardt, L. Tong, S. B. Kim, L. Eisenach, A. W. Valle, D. Hardee, R. G. Gordon, M. J. Aziz, M. P. Marshak, Science **2015**, 349, 1529.
[2]   D. G. Kwabi, K. Lin, Y. Ji, E. F. Kerr, M.-A. Goulet, D. De Porcellinis, D. P. Tabor, D. A. Pollack, A. Aspuru-Guzik, R. G. Gordon, M. J. Aziz, Joule **2018**, 2, 1894.
[3]   A. J. Esswein, J. Goeltz, D. Amadeo United States, US patent US20140051003A1, **2014.**
[4]   Wendlandt, A. E. and Stahl, S. S. (**2016**). "Quinones in Hydrogen Peroxide Synthesis and Catalytic Aerobic Oxidation Reactions." In Stahl, S. S. and Alsters, P. L. (Eds.), Liquid Phase Aerobic Oxidation Catalysis: Industrial Applications and Academic Perspectives (1st ed.) (pp. 221-237). Weinheim, Germany: Wiley-VCH Verlag GmbH & Co. KGaA.
[5]   H. N. Po, N. M. Senozan, J. Chem. Educ. **2001**, 78, 1499.
[6]   M.-A. Goulet, M. J. Aziz, J. Electrochem. Soc. **2018**, 165, A1466.